Insights into the mechanism of microtubule stabilization by Taxol

Hui Xiao*†, Pascal Verdier-Pinard†‡§, Narcis Fernandez-Fuentes†¶, Berta Burd‡, Ruth Angeletti*, Andras Fiser¶, Susan Band Horwitz‡‖, and George A. Orr‡**

Departments of ‡Molecular Pharmacology, §Obstetrics & Gynecology and Women's Health, and ¶Biochemistry, and *Laboratory of Macromolecular Analysis and Proteomics, Albert Einstein College of Medicine, Bronx, NY 10461

This contribution is part of the special series of Inaugural Articles by members of the National Academy of Sciences elected on May 3, 2005.

Contributed by Susan Band Horwitz, May 5, 2006

The antitumor drug Taxol stabilizes microtubules and reduces their dynamicity, promoting mitotic arrest and cell death. Upon assembly of the α/β-tubulin heterodimer, GTP bound to β-tubulin is hydrolyzed to GDP reaching a steady-state equilibrium between free tubulin dimers and microtubules. The binding of Taxol to β-tubulin in the polymer results in cold-stable microtubules at the expense of tubulin dimers, even in the absence of exogenous GTP. However, there is little biochemical insight into the mechanism(s) by which Taxol stabilizes microtubules. Here, we analyze the structural changes occurring in both β- and α-tubulin upon microtubule stabilization by Taxol. Hydrogen/deuterium exchange (HDX) coupled to liquid chromatography–electrospray ionization MS demonstrated a marked reduction in deuterium incorporation in both β-and α-tubulin when Taxol was present. Decreased local HDX in peptic peptides was mapped on the tubulin structure and revealed both expected and new dimer–dimer interactions. The increased rigidity in Taxol microtubules was distinct from and complementary to that due to GTP-induced polymerization. The Taxol-induced changes in tubulin conformation act against microtubule depolymerization in a precise directional way. These results demonstrate that HDX coupled to liquid chromatography–electrospray ionization MS can be effectively used to study conformational effects induced by small ligands on microtubules. The present study also opens avenues for locating drug and protein binding sites and for deciphering the mechanisms by which their interactions alter the conformation of microtubules and tubulin dimers.

hydrogen/deuterium exchange

Tubulin is a heterodimer formed by an α-subunit and β-subunit that share 40% sequence identity but almost identical three-dimensional structures (1). Tubulin polymerizes into microtubules whose functions in eukaryotic cells are responsible for mitosis, motility, maintenance of cell shape, and intracellular trafficking of macromolecules and organelles (2). Microtubules result from the head-to-tail longitudinal self-assembly of tubulin dimers to form protofilaments that interact laterally to constitute the wall of microtubules. This process is driven by GTP binding and hydrolysis at the exchangeable (E-site) of β-tubulin. GTP binds also to α-tubulin; however, it is nonexchangeable (N-site). Microtubules exhibit a highly dynamic behavior that is essential to carrying out their functions, and they undergo rapid and stochastic transitions from growing to shrinking phases resulting in a dynamic exchange of tubulin dimers at microtubule ends (3). Taxol, an effective anticancer drug, binds stoichiometrically and specifically to the β-tubulin subunit in microtubules (4) (see Fig. 5, which is published as supporting information on the PNAS web site). The resulting microtubules are stable and resist depolymerization by Ca^{2+}, cold temperature, and dilution (5). The highly dynamic behavior of microtubules is greatly suppressed by subnanomolar concentrations of Taxol, which induce abnormal mitosis and lead to cell death (6). At higher concentrations, Taxol also induces bundling of microtubules in interphase cells.

The structure of the tubulin dimer bound to Taxol at a 3.5-Å resolution was obtained by electron crystallography of zinc-induced tubulin sheets (7). Each monomer contains three major structural domains (see Figs. 6 and 7, which are published as supporting information on the PNAS web site). The N-terminal domain includes a nucleotide binding site and six parallel β-strands (S1–S6) alternating with the same number of α-helices (H1–H6). The central domain is comprised of mixed β-strands (S7–S10) and three helices (H8–H10) that are connected to the N-terminal domain by the core helix H7 and contains the hydrophobic Taxol binding pocket. The C-terminal domain is formed by two antiparallel helices (H11 and H12) crossing over the other two domains. The last 10 and 18 residues in α-tubulin and β-tubulin, respectively, are not visible in this model because they form unstructured flexible arms (7). Docking of this tubulin model in an 8-Å resolution lattice reconstructed from cryoelectron microscopy images of microtubules indicated the nature of interdimer contacts within and between protofilaments (8). In this model, the major lateral contacts occur between the M loops of one dimer and the H1–S2 loops of the dimer present in the adjacent protofilament. Although photoaffinity labeling (9) and electron crystallography (1) have localized the binding pocket for Taxol to a small region in β-tubulin, neither of these approaches gives access to conformational changes occurring in tubulin that are indicative of the mechanisms involved in microtubule stabilization, upon binding of Taxol.

To define the conformational changes that occur in tubulin upon Taxol binding, we mapped the regions displaying altered levels of hydrogen/deuterium exchange (HDX). By comparing the maps generated with GDP dimers (DIMER), GTP-induced microtubules (GTP-MT), and Taxol-stabilized microtubules (TX-MT), we identified the changes associated with Taxol binding and microtubule stabilization. The coupling of HDX with liquid chromatography–electrospray ionization (LC-ESI) MS enabled us to locate regions of Taxol-induced rigidity and Taxol-stabilized interdimer interactions.

Results and Discussion

Global HDX in Tubulin Heterodimers and Microtubules. The structure of the tubulin dimer and its docking in microtubule models have

Conflict of interest statement: No conflicts declared.

Abbreviations: HDX, hydrogen/deuterium exchange; LC-ESI, liquid chromatography–electrospray ionization; MS/MS, tandem MS; MT, microtubule; TX-MT, Taxol-stabilized MT.

See accompanying Profile on page 10163.

†H.X., P.V.-P., and N.F.-F. contributed equally to this work.

‖To whom correspondence should be addressed at: Department of Molecular Pharmacology, Albert Einstein College of Medicine, Golding 201, 1300 Morris Park Avenue, Bronx, NY 10461. E-mail: shorwitz@aecom.yu.edu.

**Deceased November 3, 2005.

predicted that once GTP is hydrolyzed, tubulin adopts a "straight" conformation and potential energy is stored in the microtubule lattice (10). Upon depolymerization, this energy is freed and the dimers adopt a relaxed "curved" conformation resulting from a kink at the intradimer interface (10). Taxol has been predicted to strengthen both longitudinal and lateral interdimer interactions thereby stabilizing microtubules (11). These effects imply distal conformational effects of GTP hydrolysis and Taxol binding to microtubules. Here, changes in flexibility of tubulin structure and dimer–dimer interactions upon binding of Taxol to microtubules were deduced from MS-based analysis of differences in the degree of deuterium incorporation into amide bonds of GDP-containing dimers (DIMER) and of microtubules assembled either in the presence of GTP alone (GTP-MT) or in the presence of both GTP and Taxol (TX-MT). D_2O itself stabilizes tubulin against denaturation (12), prevents dilution-induced depolymerization of microtubules, and suppresses their dynamicity (13). Therefore, during HDX experiments, D_2O helped to prevent tubulin unfolding and excessive depolymerization of GTP-MT during dilution in D_2O. To eliminate any ambiguity in the assignment of measured masses and potential conformational differences between different tubulin isotypes, the study was performed on chicken erythrocyte tubulin that is made up of only α1-tubulin and βVI-tubulin isotypes (see Fig. 6 for tubulin model and Fig. 7 for secondary structures) with very limited posttranslational modifications (14). Chicken βVI is 90% identical to human βI, the major β-isotype in nonneuronal cell lines, when the highly divergent C termini are not considered. The critical concentration for assembly of chicken erythrocyte tubulin is lower than brain tubulin (15) and similar to that of tubulin from human HeLa cells (16). These chicken α- and β-tubulins have 430 and 425 exchangeable amide protons, respectively, after correction for the number of proline residues (which lack exchangeable amide hydrogen atoms). After 100 min of HDX with tubulin GDP dimers, 207 (48%) and 221 (52%) of the amide hydrogens in the α- and β-tubulin chains, respectively, were replaced by deuterium. When tubulin polymerization was induced in the presence of GTP, similar extensive HDX was observed (48% in both α- and β-tubulin) (see Fig. 8*A*, which is published as supporting information on the PNAS web site). The fact that tubulin was not significantly more protected against HDX during GTP-induced polymerization is due to the continuous dynamic exchange of tubulin dimers in microtubules. Over the period required to perform the experiment, almost all of the accessible amide hydrogens can be exchanged for deuterium; an exception would be the persistence of small intermediate polymers. We speculate that such small polymers, if they exist, would be GTP-loaded and contain mostly straight dimers based on the local HDX data presented in this paper. After Taxol-induced polymerization, the exchange of tubulin dimers in microtubules stops, and polymerization continues at the expense of the pool of free tubulin dimers. This resulted in a marked reduction in deuterium incorporation with only 161 (37%) and 157 (37%) of the amide hydrogens replaced by deuterium in the α- and β-tubulin chains, respectively (Fig. 8*A*). Thus, after Taxol-induced polymerization, 46 and 64 amide hydrogens in α- and β-tubulin, respectively, were protected from deuteration due to either decreased solvent accessibility or a more rigid conformation in both polypeptide chains. In the β-tubulin chain this may reflect, in part, proximal and distal additional steric occlusion of specific amide hydrogens by Taxol, whereas in α-tubulin, it must result from long-range allosteric effects. During GTP-dependent polymerization of tubulin into microtubules, a smaller reduction in flexibility was observed on the β-chain compared with when Taxol was present (Fig. 2).

Similar observations were reported when metabolic incorporation of deuterium into tubulin was measured in tumor-bearing mice treated with Taxol (17). When Taxol was injected before D_2O, it stabilized microtubules in tumor cells and thereby prevented fast incorporation of newly deuterated tubulin into microtubules. We also observed the presence of stable microtubule bundles in peripheral blood mononuclear cells and tumor cells in patients treated with an analog of epothilone B, a microtubule-stabilizing drug that binds in the same pocket as Taxol (18). Therefore, the present *in vitro* study of mechanism(s) driving the stabilization of microtubules by Taxol has relevance to its clinical activity.

Local HDX in Peptic Peptides from Tubulin Heterodimers. Chicken tubulin heterodimers were subjected to HDX, and after quenching at low pH at different times, pepsin digestion of tubulins generated a large number of overlapping peptides, of which 210 were identified by LC-ESI tandem MS (MS/MS). This number was reduced to 112 due to the broadening of some mass peaks caused by partial deuterium incorporation. Equal numbers of peptides, 56, from α- and β-tubulin covered 81% and 91% of their sequence, respectively (see Fig. 7), and were observed consistently from tubulin dimers either free or incorporated into microtubules. Redundant peptides were eliminated, and the HDX data were plotted from 30 of 56 and 28 of 56 α- and β-tubulin peptides, respectively (Fig. 1). Various peptic peptides derived from α- and β-tubulin exhibited widely differing extents of HDX for each of the three different states of tubulin (see Figs. 8*B* and 9, which are published as supporting information on the PNAS web site). The resolution of the method reached five amino acid residues with an average of 11.7 ± 4.4 residues (range of 5–26 residues). The 35-min time point for HDX was chosen for the remaining data presented because for all peptides, this was the earliest time point when HDX reached a steady-state equilibrium. The deuterium levels of these peptides ranged from as low as 5% to >80%. To assess local protection against HDX, we calculated the HDX ratio of DIMER to GTP-MT and DIMER to TX-MT, and of GTP-MT to TX-MT. Such calculations cancelled out the effects due to D_2O alone and, more importantly, revealed the Taxol-specific changes of HDX in tubulin (Fig. 2). For example, peptide α243–248 (H7–H8 loop) with a HDX ratio of DIMER to GTP-MT or DIMER to TX-MT of 1.56 (Fig. 1*A*) appears in yellow when mapped on the tubulin heterodimer model (Fig. 2 *A* and *B*). The αH7–H8 loop participates in the hydrolysis of GTP on β-tubulin upon assembly (19); therefore, it is consistent that it be protected against HDX when tubulin is polymerized. This effect was specific for GTP because the ratio of TX-MT to GTP-MT was 1 (dark gray in Fig. 2*C*). Otherwise, GTP-induced protection from HDX was limited to two other regions, H10 (β324–330) and the H9–S8 loop (β294–303) of β-tubulin, which became even more protected when Taxol was present (Figs. 1*B* and 2).

Mechanism by Which Taxol Stabilizes Microtubules. As expected, the binding pocket for Taxol as well as proximal regions were protected upon the binding of Taxol to microtubules. For example, peptide β212–230 was protected (Fig. 1*B*; yellow in Fig. 2 *A* and *C* and Fig. 3), and mutation of leucine residues in this region is associated with altered sensitivity to Taxol (20). The protection of the region located at the GDP binding site on β-tubulin (β133–151) was also evident (Fig. 2 *A* in orange, *B* in yellow, and *C* in dark gray) and was due to the entrapment of exchangeable GTP/GDP between dimers when they are incorporated into microtubules. On α-tubulin, the S-loop, which occupies the equivalent binding pocket for Taxol on β-tubulin, is slightly protected upon microtubule assembly (peptide α368–376; Figs. 1*A* and 2*A*) and stabilization by Taxol (α352–368; Fig. 2 *A* and *C*). Therefore, the α-tubulin region located at exactly the same position as Taxol on β-tubulin may lose flexibility as well as accommodate a uniform reduction of the distance between

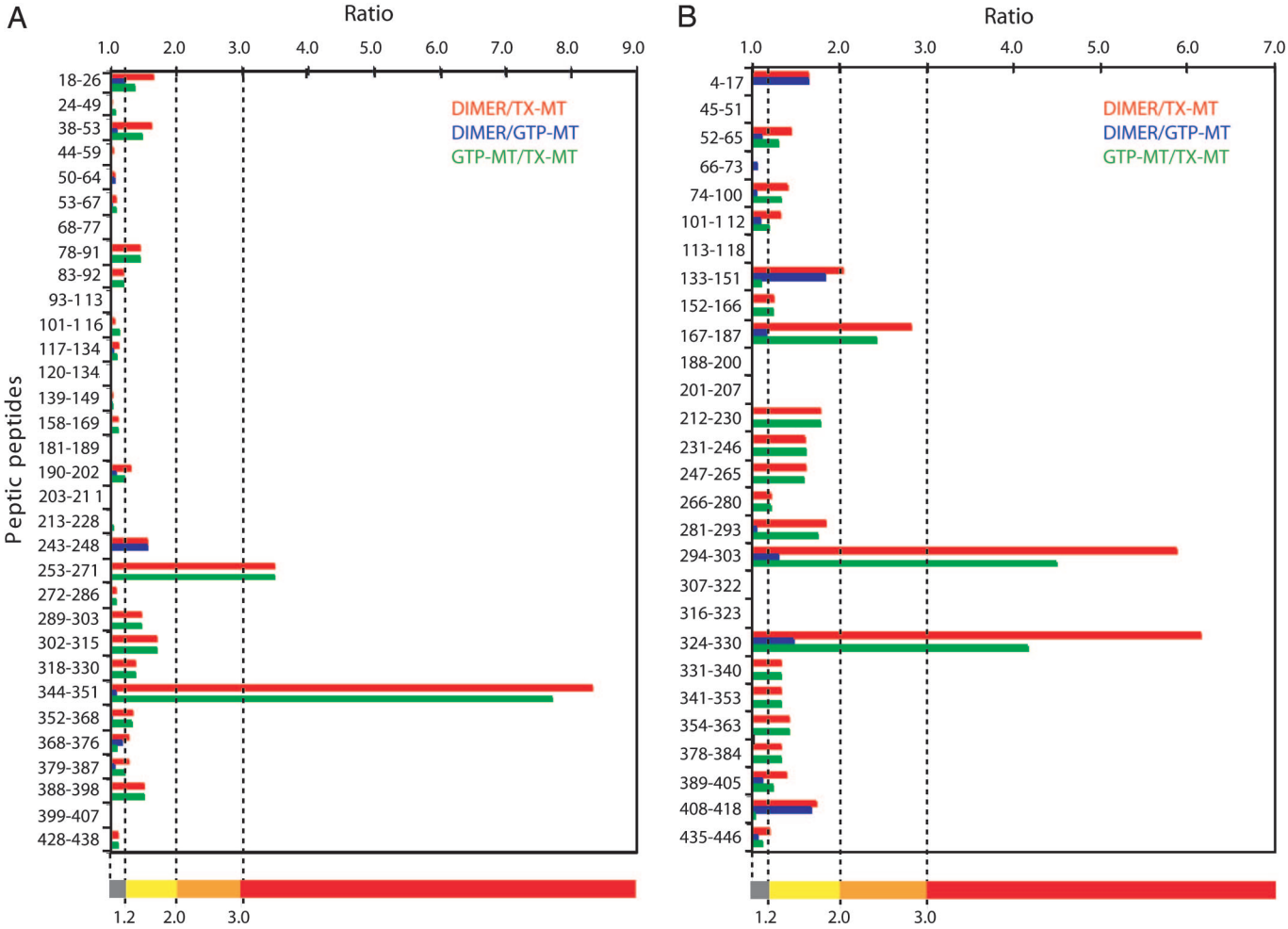

Fig. 1. Ratios of percentages of HDX in peptic peptides along the sequence of tubulin. The bar diagrams show relative HDX in the three systems studied: tubulin dimer (DIMER), TX-MT, and microtubules polymerized in the presence of GTP alone (GTP-MT). Ratios of HDX percentages of peptic peptides at 35 min from α-tubulin (*A*) and from β-tubulin (*B*) are represented for DIMER to TX-MT as red bars, DIMER to GTP-MT as blue bars, and GTP-MT to TX-MT as green bars. The first and last residues of each peptide are indicated on the left axis from the N terminus at the top to the C terminus. Ratio values are indicated on the top horizontal axis. The bottom colored bar indicates the color-coding of the HDX ratio (r) that is used for the models in Figs. 2 and 3 (dark gray, $r \leq 1.2$; yellow, $1.2 < r \leq 2.0$; orange, $2.0 < r \leq 3.0$; red, $r > 3$).

H1–S2 and M loops along a quasi vertical axis. A small region, α18–24 (H1), forms the bottom of a groove running along the longitudinal axis of protofilaments on the inside of the microtubule. It was also more protected when Taxol was present (Figs. 1*A* and 2), indicating that regions contiguous with H1 tend to close in on each other upon microtubule assembly and stabilization by Taxol. Taxol reduces the average number of protofilaments forming a microtubule from 13, in taxane-free or Taxotere microtubules, to 12 (21). This finding suggests that binding of Taxol must decrease the distance between the H1–S2 and M loops, therefore closing the angle between dimers in adjacent protofilaments from 152.3° to 150° (21). Because Taxotere does not have this effect on the microtubule lattice but stabilizes microtubules like Taxol, HDX experiments with Taxotere will afford further dissection of these conformational changes in tubulin.

Keskin *et al.* (22) hypothesized that a lateral compression of tubulin dimer is coupled with a longitudinal expansion of the dimer. Indeed, peptide α344–351 (C-terminal of H10–S9 loop), upstream of the S-loop, and the contiguous peptide α253–271 (H8 + H8–S7 loop + S7) were greatly protected from HDX upon Taxol binding (peptides ⑤ and ④, respectively, in Fig. 3), which is consistent with a gain in strength of longitudinal interdimer contacts (23) and in microtubule rigidity (24). This result implied that Taxol has a strong allosteric effect on α-tubulin. These α-tubulin regions are in contact with peptide β167–187 at the interdimer interface, which was also highly protected against HDX when Taxol was present (orange in Figs. 2 and 3; peptide ① in Fig. 3). Mutation V260I in yeast α-tubulin was recently reported to inhibit microtubule dynamics and to activate the spindle checkpoint (25). Moreover, phosphorylation of βSer172 by the cyclin-dependent kinase Cdk1 prevents the incorporation of tubulin into mitotic microtubules (26). This observation was interpreted, after modeling, as resulting from an inhibition of GTP binding and/or of interdimer interactions. Peptide β167–187 was not protected against HDX upon binding of GTP (Figs. 2*B* and 3*B*), indicating that βSer172 is more involved in interdimer interactions than binding of GTP.

At the intradimer interface, a β-tubulin peptide from residues 247 to 265 (C-terminal of H7–H8 loop + H8 + H8–S7 loop) was more protected from HDX in the presence of Taxol but to a lesser extent than the downstream peptide β324–330 (H10) (Fig. 3*D*). This observation is in agreement with the transition from a curved unpolymerized conformation to a straight conformation of the dimer upon GTP binding and incorporation into the microtubule lattice. No such change was seen on the opposite

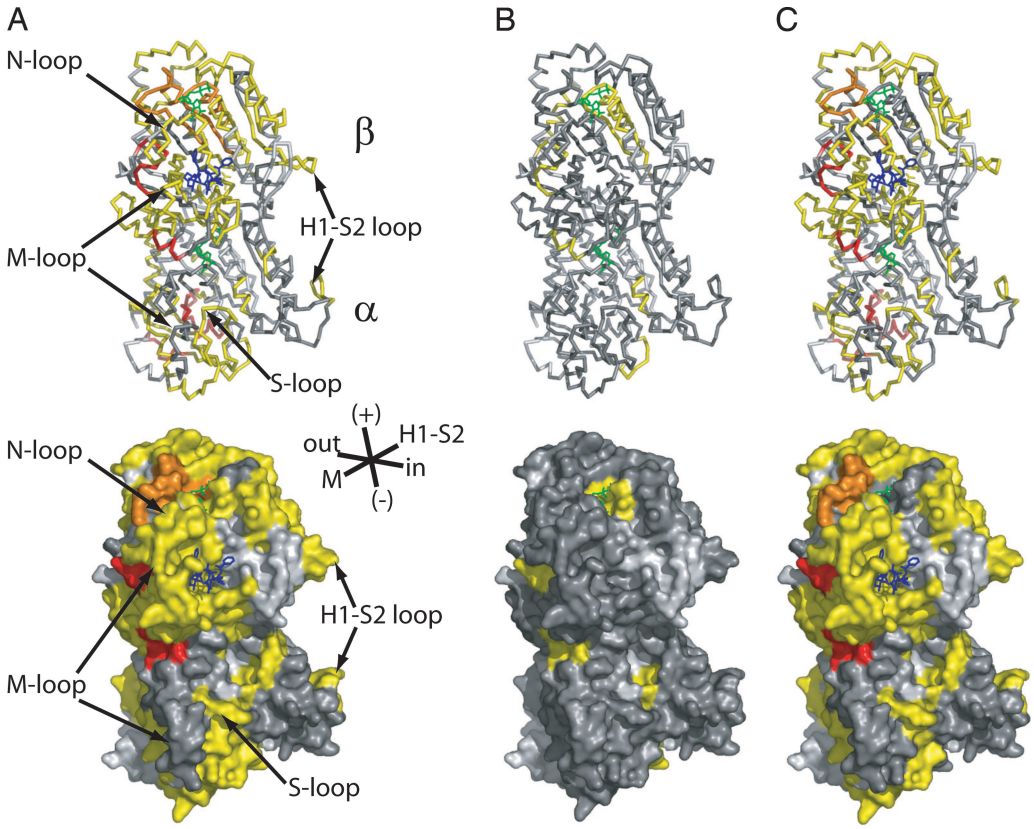

Fig. 2. Mapping HDX ratio changes on the tubulin model. (*A*) DIMER to TX-MT. (*B*) DIMER to GTP-MT. (*C*) GTP-MT to TX-MT. (*Upper*) Tubulin structure as ribbons. (*Lower*) Molecular surface of tubulin. Peptic peptides are colored according to the code indicated in Fig. 1, and light gray areas are due to missing peptides.

side of the intradimer interface (H1–S2 loop side), thus indicating that the dimer straightens in the direction of H10. This effect is directly connected to the protection of peptides β231–246 (C-terminal half of H7 + two-thirds of H7–H8 loop) and β212–230 (H6–H7 loop + N-terminal half of H7) due to the binding of Taxol in the pocket formed by these peptides and the M loop (Figs. 1*B* and 2).

We found three peptides in β-tubulin, β4–17, β133–151, and β408–418, that were protected to a similar extent in GTP-MT and TX-MT (Fig. 1*B*). Peptides β4–17 and β133–151 are in the core of β-tubulin and are not exposed at the surface, and their respective strands, S1 and S4, are in close contact. This finding is consistent with a gain in rigidity of the α/β-tubulin heterodimer upon assembly into microtubules. The immediate downstream peptide β152–166, comprising the last third of H4, the H4–S5 loop, and half of H5, is exposed on the lateral surface (H1–S2 loop side) and displayed a small decrease in accessibility to HDX in the presence of Taxol (Fig. 1*B*, yellow in Figs. 2*C*, and peptide ⑥ in Fig. 3). Peptide β408–418 (H12) is located at the surface of the microtubule and participates in the binding of MAPs (microtubule-associated proteins) (27). In this instance, despite the high purity of our tubulin preparation, we cannot exclude the possible presence of trace amounts of contaminating MAPs that could protect this region from HDX.

M loops in α- and β-tubulin have been predicted, by modeling, to be involved in lateral interactions with the H1–S2 loops of the adjacent dimer (8). Peptide β281–293 consisting of the C terminus of the M loop and of H9 appears in yellow in Fig. 2 *A* and *C* and Fig. 3. The downstream peptide, β294–303 (H9–S8 loop; Fig. 1*B*), like H10, was highly protected when microtubules were stabilized by Taxol (yellow in Fig. 2*B*, red in Fig. 2 *A* and *C*, and red in Fig. 3). Therefore, the M loop of β-tubulin appeared to gain in rigidity while being surrounded by two highly protected regions, a situation resulting most likely from the straightening of the dimer upon assembly into microtubules. Interestingly, there was no such effect observed on the α-tubulin M loop, indicating that most of the stabilization of lateral contacts by Taxol occurs in the near vicinity of its binding to β-tubulin. This result is in agreement with predictions by Keskin *et al.* (22), using a computational approach. Our modeling of microtubule protofilaments (Fig. 3 *A* and *B*) was based on the chicken erythrocyte tubulin model (see Fig. 6). We were able to observe the potential discreet lateral contacts between adjacent protofilaments. Of particular interest is the αLys40, which is one of the six residues of the αH1–S2 loop protected against HDX in the presence of Taxol. Lys-40 is embedded in the lateral contacts of adjacent α-tubulins. Its side chain was pointing out toward the back of the adjacent M loop. This residue is acetylated in stable microtubules in cells by a yet unidentified acetyl transferase (28), and its acetylation is increased when cells are treated with Taxol and other microtubule-stabilizing drugs. Deacetylation is performed by the histone deacetylase 6 (HDAC6) (29) whose inhibition by small inhibitors, such as trichostatin A, results in an increase of tubulin acetylation (30). We have found that an increase of tubulin acetylation depends on the dose of Taxol (P. Verdier-Pinard and S.B.H., unpublished observations), and three hypotheses can be considered: Taxol directly inhibits HDAC6 in a manner similar to trichostatin A, HDAC6 is inhibited by Taxol-microtubules, or the acetylated Lys-40 becomes less accessible to HDAC6 upon stabilization of microtubules. Our data favor the latter hypothesis. The contacts between adjacent α-tubulins appeared to be potentially weaker than the one between adjacent β-tubulins, because the M loops in α-tubulin were more flexible in the presence of Taxol. Therefore, the Lys-40 side chain may flip out of the lateral interface between α-tubulins with a decreasing frequency as microtubules are

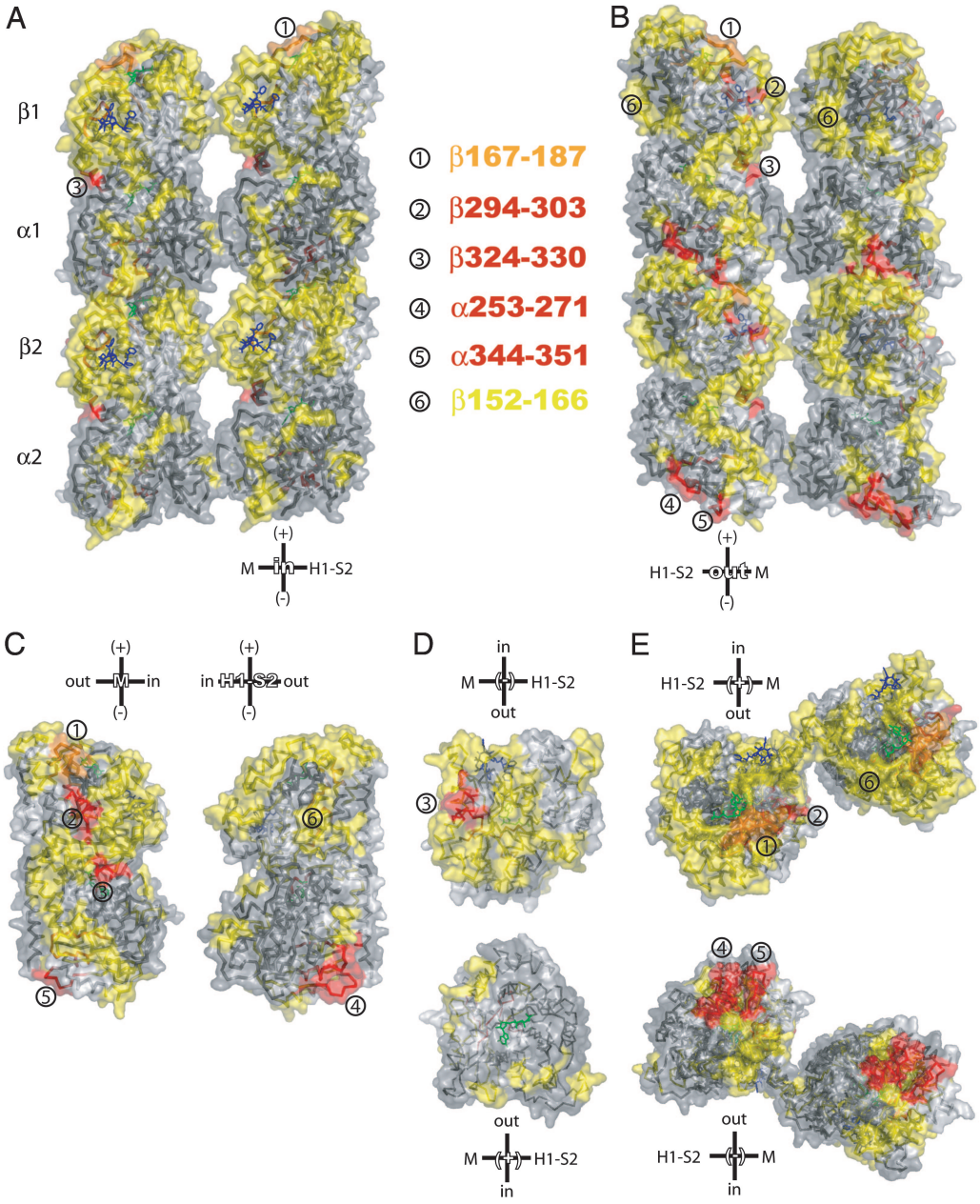

Fig. 3. Mapping of the HDX ratio, GTP-MT to TX-MT, on a microtubule model. The extent of protection against HDX is color-coded as in Figs. 1 and 2. (*A*) View of a portion of two adjacent protofilaments from inside to outside in a microtubule. The right protofilament is facing the viewer, whereas the left one is coming toward the viewer. (*B*) View of a portion of two adjacent protofilaments from outside to inside of a microtubule. The left protofilament is facing the viewer, whereas the right one is going away from the viewer. (*C*) Lateral interfaces of dimers. (*D*) Intradimer interface with β-tubulin at the top and α-tubulin at the bottom. (*E*) Interdimer interfaces in protofilaments. (*Upper*) View of protofilaments in *B* from the top (β-tubulin). (*Lower*) View of protofilaments in *B* from the bottom (α-tubulin). Lateral relative orientation of dimers is based on a TX-MT made of 12-protofilaments. Taxol is in blue, and GDP is in green. The surfaces were superimposed by transparency on the ribbon structures. Some of the peptides that are discussed in the text are numbered, and their location is indicated on the different views of the HDX map.

stabilized by increasing concentrations of Taxol. Thus, the acetylated side chain would become less accessible as the lateral contacts between α-tubulins become less labile. It is also possible that the acetylated side chain of αLys40 becomes part of the lateral contacts and participates in its stabilization. The present study confirmed experimentally that M and H1–S2 loops participate in lateral contacts between protofilaments.

When the lateral surfaces of adjacent dimers were compared (Fig. 3*C*), the HDX map of peptide β152–166 (peptide ⑥) is almost the mirror image of the HDX map generated by the immediate downstream peptide β167–187 (peptide ①), and peptides β294–303 and β324–330 (peptides ② and ③, respectively). Noticeably, a mirror HDX map (yellow in Fig. 3*C*) on the M loop side is clearly visible. Therefore, the entire region spanning from β133 to β187 appeared to be affected by Taxol on both lateral faces of the dimer. The cryoelectron microscopy reconstruction of guanylyl-(α,β)-methylene-diphosphonate-tubulin tubes presented by Wang and Nogales (31) suggested that protofilaments are associated by microtubule-like lateral contacts to form pairs and that these pairs are associated with each

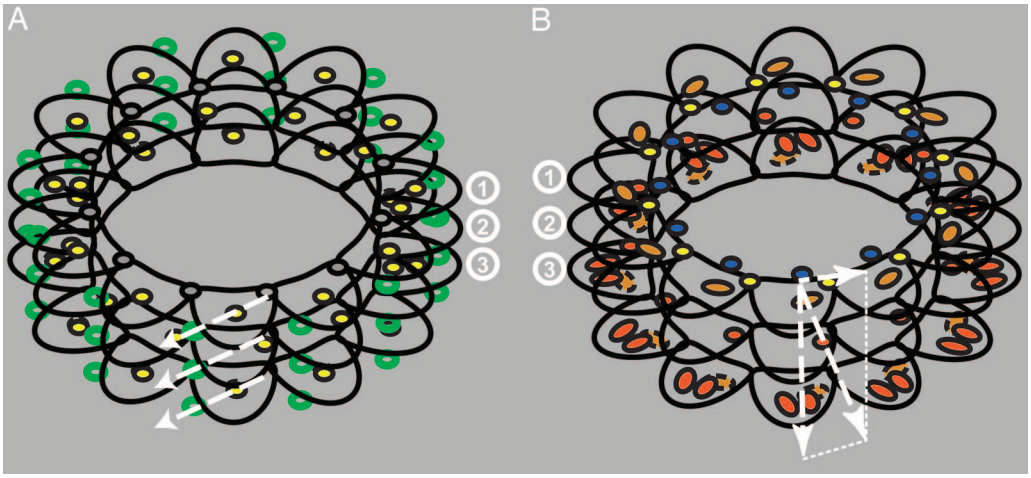

Fig. 4. Diagrams of HDX results at the interfaces of tubulin dimers in microtubules. (*A*) Diagram of HDX ratio, DIMER to GTP-MT, with stathmin (green circles) bound to the outside of the microtubule. The lateral contacts are represented as gray discs; longitudinal contacts and H10 at the inter- and intradimer, respectively, are represented as yellow discs. Depolymerizing outward forces are represented by white dashed arrows. (*B*) Diagram of HDX ratio GTP-MT to TX-MT with Taxol (blue discs) bound to the inside of the microtubule. Lateral contacts and H10 are represented as yellow and red discs, respectively. Peptide β167–187 is represented as orange ovals, and peptides α253–271 and α344–351 are represented as red ovals, at the top of β-tubulin and at the bottom of α-tubulin, respectively. Longitudinal, lateral, and resultant forces induced by Taxol stabilization are represented by dashed white arrows. Superimposition of the top of β-tubulin with the bottom of α-tubulin is represented by dashed ellipses. For simplification and to help visualize the superimposition of GTP and Taxol contributions to the establishment of longitudinal and lateral contacts, the microtubule in *A* is made only of 12-protofilaments as in *B* where Taxol is present. Distances between interfaces in *B* have been slightly increased to represent the dimer longitudinal expansion induced by Taxol. ①, top of β-tubulin plus lateral contact; ②, intradimer interface; ③, bottom of α-tubulin plus interdimer interface.

other by the middle portions of the two faces of the lateral interface. They proposed that this alternate pattern of lateral contacts is an intermediate form of protofilament association involved in the closure of the microtubule wall that would require a "roll in" by a 60° rotation of the contacts between two pairs of protofilaments. Remarkably, the two HDX maps presented in Fig. 3*C* and discussed above match these alternate lateral interactions. We speculate that Taxol induces a loss of flexibility of the involved regions that prevents a "roll out" of lateral contacts in microtubules that would otherwise open up their wall.

Our most significant results on HDX analysis by mass spectrometry on tubulin dimers and microtubules stabilized by Taxol are summarized in Fig. 4. In the absence of Taxol, it is predicted that the energy stored in longitudinal contacts is greater than that stored in lateral contacts (32). From the present study, we conclude that Taxol is increasing those energies while maintaining the same differential between lateral (Fig. 4*B*, short horizontal arrow) and longitudinal (Fig. 4*B*, long vertical arrow) contacts in the microtubule lattice. Consequently, a pressure is specifically applied on βH10 at the intradimer interface (Fig. 4*B*, long slanted arrow), maintaining dimers in a straight conformation. Inversely, in depolymerizing conditions, weak lateral and stronger longitudinal bonds are completely and partially disrupted, respectively, and dimers adopt a curved conformation and protofilaments peel outwards in a lateral motion (Fig. 4*A*, long slanted arrows). Our rational is based on the facts that (*i*) this would efficiently disrupt lateral bonds; (*ii*) stathmin, a microtubule destabilizing protein, binds on the outside of the microtubule diametrically opposite from M loop and H10 (Fig. 4*A*, green circles) (33); and (*iii*) colchicine and vinblastine bind at the intra- and interdimer interface, respectively, between the center of the interface and H10 of the M loop (34). Thus, stathmin on the outside of the microtubule acting as a "spring" pulling dimers outward or colchicine and vinblastine acting as "levers" on the inside of the microtubule would bend protofilaments in the same direction. Moreover, motors such as kinesins walk on the external crest of protofilaments and do not act on microtubule stability (35) whereas MAPs such as Tau bind near the lateral contacts and potentially at the Taxol binding site and stabilize microtubules (36). These views are in strong agreement with the recent publication by Wang and Nogales (31) that suggests a regulation of tubulin dimer bending by GDP in the same outward direction.

The present study indicates that HDX coupled to MS can give insights into the conformational changes induced in tubulin by drugs. Such information will help us to understand the molecular mode of action of these drugs. Access to precise kinetic data of protection against or exposure to HDX will be important to refine our observations with Taxol and assess subtle differences with other microtubule-stabilizing agents. These analyses will answer important pharmacological and biochemical questions relevant to the function of microtubules in cells and expand our knowledge of a group of drugs that are important in cancer chemotherapy.

Materials and Methods

Materials. Pepsin was purchased from Sigma-Aldrich, D_2O (99.9%) was purchased from Cambridge Isotope Laboratories, trifluoroacetic acid was purchased from Applied Biosystems, and acetonitrile was purchased from Fisher Scientific. GDP and GTP were purchased from Roche. All other chemicals were of highest grade commercially available from Sigma-Aldrich. Tubulin was isolated from the marginal bands of chicken erythrocytes by the method of Murphy (15). It contains a single α- and β-isotype, α1 and βVI, whose amino acid sequences are 95% and 84% identical to their human orthologs, respectively. Purity was 99% as evaluated by SDS/PAGE and Coomassie staining, and isotype content was checked by high-resolution isoelectric focusing (37). The tubulin stock solution at 15 mg/ml was stored at −80°C.

Hydrogen to Deuterium Exchange. All tubulin samples were clarified by centrifugation at 100,000 × *g* and 4°C for 10 min before assembly. For GTP-induced assembly, tubulin was incubated at 6.0 mg/ml (10 times the critical concentration for assembly)

in MEM buffer (0.1 M 2-morpholinoethane sulfonic acid/1 mM EGTA/0.5 mM $MgCl_2$, pH 6.9) at 37°C in the presence of 1 mM GTP for 30 min. When Taxol was present, 10 μM was added after a 15-min preincubation of GTP-MT and incubation was continued for 15 min. GDP-tubulin dimers (DIMER) were prepared in the same MEM buffer, but in the presence of 1 mM GDP at room temperature for 30 min. HDX on tubulin was initiated by diluting either the microtubule or dimer preparation 20-fold into deuterated MEM buffer, pD 7.0 at 37°C. The deuterated buffer contained either 1 mM GTP or 1 mM GTP plus 10 μM Taxol or 1 mM GDP in which GTP-MT, TX-MT, or DIMER were diluted. At the indicated times, samples were subjected to both global and local HDX. Aliquots of exchange solution were quenched by adding equal volumes of 0.5 M phosphate buffer (pH 2.5), followed by immediate LC-ESI MS analysis for global HDX experiments or by an additional 5-min pepsin digestion at 0°C and subsequent LC-ESI MS/MS analysis for local HDX experiments.

LC MS and LC MS/MS Analysis. The extent of deuterium incorporation into tubulin or proteolytic peptides was determined by LC-ESI MS. A Shimadzu HPLC equipped with two LC-10AD pumps was used to generate a fast gradient with a 50 μl/min flow rate. Solvent A was a mixture of 95% H_2O, 4.95% acetonitrile, and 0.05% trifluoroacetic acid, and solvent B was 95% acetonitrile mixed with 4.95% H_2O and 0.05% trifluoroacetic acid. To minimize the back-exchange during HPLC, the solvent precooling coil, static mixing tee, Rheodyne injector, and column were immersed in an ice bath. Aliquots of exchanging protein solution (5 μl) or peptic peptides (20 μl) were quenched and loaded onto a C3 (MicroTech Scientific, Vista, CA) or C8 (Vydac, Hesperia, CA) column with a dimension of 1.0 $\times$ 50 mm. Allowing a 5-min desalting with 5% solvent B, the intact protein was eluted with a 2-min gradient from 5% to 95% solvent B, and peptic peptides were eluted with a 0.5-min gradient from 5% to 10% B, followed by an 8-min gradient from 10% to 50% solvent B. The 50 μl/min non-split effluent was delivered into a LTQ mass spectrometer (Thermo Electron Corporation). The LTQ mass spectrometer was operated in a data-dependent mode containing three-event scans (a full mass scan, a zoom scan, and an MS/MS scan). Peptides were identified by searching against a tubulin database with MASCOT and SQUEST combined with manual interpretation. The percentage of deuterium in peptic peptides was determined from the mass difference between nondeuterated and deuterated samples without adjustment of deuterium gain or loss during peptic digestion and subsequent LC-ESI MS analysis. The effect of deuterium gain or loss is not taken into account in this work because we compare the HDX ratio of three forms of tubulins under identical conditions. The standard deviation determined by replicates is <15%. The significant changes in HDX ratio were set at 1.2 (yellow). The color-coding of the HDX ratio (r) that is used in this paper is as follows: dark gray, $r \leq 1.2$; yellow, $1.2 < r \leq 2.0$; orange, $2.0 < r \leq 3.0$; red, $r > 3$.

Model of Taxol Bound Erythrocyte Chicken Tubulin Protofilaments. A protein structure model of chicken erythrocyte tubulin dimer was constructed with MODELLER (38) by using the structure of a bovine brain tubulin in complex with Taxol [Protein Data Bank entry 1TUB (1)] and its refined structure of bovine brain tubulin dimer in a complex with Taxol [Protein Data Bank entry 1JFF (7)] as templates. Although the crystallographic resolution of 1JFF is higher, 1TUB was also used because it includes the H1–S2 loop in the α-subunit (residue 35–60) that is missing from the 1JFF structure. The sequences used for the template files are from pig brain tubulin (7). The sequence identities between chicken erythrocyte and pig brain tubulin sequences are 90.4% and 82.2% for the α- and β-subunits, respectively. We used chicken erythrocyte tubulin to remodel the tubulin dimer (see Figs. 6 and 7). The comparative models of dimers were arranged into protofilament and microtubule forms through computational rigid-body docking, in the following way. Docked configurations of two dimers were sampled by using the program FTDOCK 2.0 (39). The sampling space was populated with 10,000 complexes that exhibited the best surface complement on the dimer interface. These complexes were rescored by using statistical pair potentials (40) and further filtered by experimentally known longitudinal and lateral contacts that were obtained from previously published experiments (8) or from the current deuterium exchange data. Top-scoring complexes of the initial crude complex configuration were refined, and the side-chain rotamer conformations were optimized by using the program MULTIDOCK (41). Finally, the best scoring complexes for lateral (microtubule) and longitudinal (protofilament) arrangements were selected and merged. The bovine tubulin dimer was structurally superimposed with the erythrocyte chicken tubulin complexes to inherit the structural orientation of Taxol, GTP, and GDP molecules. The resulting complex structure was explored with the program TURBO-FRODO (42) and further refined.

This article is dedicated to the memory of our colleague George A. Orr. This work was supported by National Cancer Institute Grants CA 083185 and CA 077263 (to S.B.H.), the National Foundation for Cancer Research (S.B.H.), and National Institutes of Health Grant NIH-NIAID-DMID-BAA-0338 (to A.F.).

1. Nogales, E., Wolf, S. G. & Downing, K. H. (1998) *Nature* **391,** 199–203.
2. Sharp, D. J., Rogers, G. C. & Scholey, J. M. (2000) *Nature* **407,** 41–47.
3. Desai, A. & Mitchison, T. J. (1997) *Annu. Rev. Cell Dev. Biol.* **13,** 83–117.
4. Diaz, J. F., Menendez, M. & Andreu, J. M. (1993) *Biochemistry* **32,** 10067–10077.
5. Schiff, P. B., Fant, J. & Horwitz, S. B. (1979) *Nature* **277,** 665–667.
6. Yvon, A. M., Wadsworth, P. & Jordan, M. A. (1999) *Mol. Biol. Cell* **10,** 947–959.
7. Lowe, J., Li, H., Downing, K. H. & Nogales, E. (2001) *J. Mol. Biol.* **313,** 1045–1057.
8. Nogales, E., Whittaker, M., Milligan, R. A. & Downing, K. H. (1999) *Cell* **96,** 79–88.
9. Orr, G. A., Verdier-Pinard, P., McDaid, H. & Horwitz, S. B. (2003) *Oncogene* **22,** 7280–7295.
10. Nogales, E., Wang, H. W. & Niederstrasser, H. (2003) *Curr. Opin. Struct. Biol.* **13,** 256–261.
11. Andreu, J. M., Bordas, J., Diaz, J. F., Garcia de Ancos, J., Gil, R., Medrano, F. J., Nogales, E., Pantos, E. & Towns-Andrews, E. (1992) *J. Mol. Biol.* **226,** 169–184.
12. Chakrabarti, G., Kim, S., Gupta, M. L., Jr., Barton, J. S. & Himes, R. H. (1999) *Biochemistry* **38,** 3067–3072.
13. Panda, D., Chakrabarti, G., Hudson, J., Pigg, K., Miller, H. P., Wilson, L. & Himes, R. H. (2000) *Biochemistry* **39,** 5075–5081.
14. Rudiger, M. & Weber, K. (1993) *Eur. J. Biochem.* **218,** 107–116.
15. Murphy, D. B. & Wallis, K. T. (1983) *J. Biol. Chem.* **258,** 7870–7875.
16. Newton, C. N., DeLuca, J. G., Himes, R. H., Miller, H. P., Jordan, M. A. & Wilson, L. (2002) *J. Biol. Chem.* **277,** 42456–42462.
17. Fanara, P., Turner, S., Busch, R., Killion, S., Awada, M., Turner, H., Mahsut, A., Laprade, K. L., Stark, J. M. & Hellerstein, M. K. (2004) *J. Biol. Chem.* **279,** 49940–49947.
18. McDaid, H. M., Mani, S., Shen, H. J., Muggia, F., Sonnichsen, D. & Horwitz, S. B. (2002) *Clin. Cancer Res.* **8,** 2035–2043.
19. Anders, K. R. & Botstein, D. (2001) *Mol. Biol. Cell* **12,** 3973–3986.
20. Gonzalez-Garay, M. L., Chang, L., Blade, K., Menick, D. R. & Cabral, F. (1999) *J. Biol. Chem.* **274,** 23875–23882.
21. Andreu, J. M., Diaz, J. F., Gil, R., de Pereda, J. M., Garcia de Lacoba, M., Peyrot, V., Briand, C., Towns-Andrews, E. & Bordas, J. (1994) *J. Biol. Chem.* **269,** 31785–31792.
22. Keskin, O., Durell, S. R., Bahar, I., Jernigan, R. L. & Covell, D. G. (2002) *Biophys. J.* **83,** 663–680.
23. Dye, R. B., Flicker, P. F., Lien, D. Y. & Williams, R. C., Jr. (1992) *Cell Motil. Cytoskeleton* **21,** 171–186.

24. Mickey, B. & Howard, J. (1995) *J. Cell Biol.* **130,** 909–917.
25. Asakawa, K., Kume, K., Kanai, M., Goshima, T., Miyahara, K., Dhut, S., Tee, W. W., Hirata, D. & Toda, T. (2006) *Mol. Biol. Cell* **17,** 1421–1435.
26. Fourest-Lieuvin, A., Peris, L., Gache, V., Garcia-Saez, I., Juillan-Binard, C., Lantez, V. & Job, D. (2006) *Mol. Biol. Cell* **17,** 1041–1050.
27. Amos, L. A. (2000) *Curr. Opin. Struct. Biol.* **10,** 236–241.
28. Westermann, S. & Weber, K. (2003) *Nat. Rev. Mol. Cell Biol.* **4,** 938–947.
29. Zhang, Y., Li, N., Caron, C., Matthias, G., Hess, D., Khochbin, S. & Matthias, P. (2003) *EMBO J.* **22,** 1168–1179.
30. Haggarty, S. J., Koeller, K. M., Wong, J. C., Grozinger, C. M. & Schreiber, S. L. (2003) *Proc. Natl. Acad. Sci. USA* **100,** 4389–4394.
31. Wang, H. W. & Nogales, E. (2005) *Nature* **435,** 911–915.
32. Van Buren, V., Odde, D. J. & Cassimeris, L. (2002) *Proc. Natl. Acad. Sci. USA* **99,** 6035–6040.
33. Gigant, B., Curmi, P. A., Martin-Barbey, C., Charbaut, E., Lachkar, S., Lebeau, L., Siavoshian, S., Sobel, A. & Knossow, M. (2000) *Cell* **102,** 809–816.
34. Ravelli, R. B., Gigant, B., Curmi, P. A., Jourdain, I., Lachkar, S., Sobel, A. & Knossow, M. (2004) *Nature* **428,** 198–202.
35. Krebs, A., Goldie, K. N. & Hoenger, A. (2004) *J. Mol. Biol.* **335,** 139–153.
36. Santarella, R. A., Skiniotis, G., Goldie, K. N., Tittmann, P., Gross, H., Mandelkow, E. M., Mandelkow, E. & Hoenger, A. (2004) *J. Mol. Biol.* **339,** 539–553.
37. Verdier-Pinard, P., Wang, F., Martello, L., Burd, B., Orr, G. A. & Horwitz, S. B. (2003) *Biochemistry* **42,** 5349–5357.
38. Sali, A. & Blundell, T. L. (1993) *J. Mol. Biol.* **234,** 779–815.
39. Gabb, H. A., Jackson, R. M. & Sternberg, M. J. (1997) *J. Mol. Biol.* **272,** 106–120.
40. Moont, G., Gabb, H. A. & Sternberg, M. J. (1999) *Proteins* **35,** 364–373.
41. Jackson, R. M., Gabb, H. A. & Sternberg, M. J. (1998) *J. Mol. Biol.* **276,** 265–285.
42. Roussel, A., Fontecilla-Camps, J. C. & Cambillau, C. (1990) *J. Mol. Graphics* **8,** 86–88, 91.